nature materials

ARTICLES

https://doi.org/10.1038/s41563-020-00841-z

Synergistically integrated phosphonated poly(pentafluorostyrene) for fuel cells

Vladimir Atanasov[1,9], Albert S. Lee[2,8,9], Eun Joo Park[2], Sandip Maurya[2], Ehren D. Baca[3], Cy Fujimoto[3], Michael Hibbs[3], Ivana Matanovic[4,5], Jochen Kerres[1,6,7] ✉ and Yu Seung Kim[2] ✉

Modern electrochemical energy conversion devices require more advanced proton conductors for their broad applications. Phosphonated polymers have been proposed as anhydrous proton conductors for fuel cells. However, the anhydride formation of phosphonic acid functional groups lowers proton conductivity and this prevents the use of phosphonated polymers in fuel cell applications. Here, we report a poly(2,3,5,6-tetrafluorostyrene-4-phosphonic acid) that does not undergo anhydride formation and thus maintains protonic conductivity above 200 °C. We use the phosphonated polymer in fuel cell electrodes with an ion-pair coordinated membrane in a membrane electrode assembly. This synergistically integrated fuel cell reached peak power densities of 1,130 mW cm^{-2} at 160 °C and 1,740 mW cm^{-2} at 240 °C under H_2/O_2 conditions, substantially outperforming polybenzimidazole- and metal phosphate-based fuel cells. Our result indicates a pathway towards using phosphonated polymers in high-performance fuel cells under hot and dry operating conditions.

There is growing international consensus that electrochemical energy conversion of clean hydrogen and high-energy-density fuel will be vital in the global transition towards a sustainable-energy future[1]. Operating proton exchange membrane fuel cells (PEMFCs) at temperatures higher than 100 °C offers several advantages, including co-generation of heat and power, high tolerance to fuel impurities and a simpler system design. The high-temperature PEMFCs (HT-PEMFCs) include the well established phosphoric-acid-doped polybenzimidazole (PA-PBI)-based HT-PEMFCs, which can operate within the temperature range 140–200 °C without humidification[2]. At present, HT-PEMFCs show limited stability in the presence of water or at higher operating temperatures. To improve stability, we have developed ion-pair coordinated membranes with strong interaction between biphosphate–ammonium ionic pairs that increase the water tolerance and reduce evaporation of phosphoric acid at high temperatures[3]. However, the performance was low compared to that of the state-of-the-art PA-PBI-based HT-PEMFCs.

Ionomeric binder materials play a critical part in the performance of polymer-based fuel cells and electrolysers. For example, the Nafion ionomer enables the catalyst loading to be reduced by 20 times with improved performance for low-temperature PEMFCs[4]. Quaternized poly(fluorene) and radiation-grafted ethylene tetrafluoroethylene binders have greatly improved the performance of alkaline membrane fuel cells in the past five years[5,6]. More recently, a highly quaternized polystyrene binder much improved the performance of a noble-metal-free alkaline anion exchange membrane water electrolyser[7]. However, advanced ionomeric binders for HT-PEMFCs have not been thoroughly investigated.

We consider phosphonated polymers as promising candidates for use as ionomeric binders. Several research groups have developed phosphonated polymers as a potential membrane for HT-PEMFCs[8–18] because of their ability to conduct protons under both hydrated and anhydrous conditions[19]. One challenge of using phosphonated polymers originates from their poor mechanical properties, caused by strong intermolecular hydrogen bonding and dipole–dipole association[20]. Another challenge is the low anhydrous proton conductivity of phosphonated polymers (<1 mS cm^{-1}) at 100–200 °C owing to the formation of phosphonic acid anhydride[21–23]. It is known that phosphonic acid anhydrides have much lower proton conductivities than phosphonic acids owing to their lower degree of hydrogen-bond-network frustration[24,25]. Therefore, no high-performance HT-PEMFCs based on phosphonated polymer membranes have been reported.

When a polymer is used as the ionomeric binder, the poor mechanical properties of phosphonated polymers may not substantially limit fuel cell performance and durability, given that the mechanical toughness of Nafion ionomers is three orders of magnitude lower than that of the Nafion membrane[26]. Owing to the relatively thin coating of ionomer used in the catalyst layer (an ionomer a few nanometres thick versus a membrane 10–20 μm thick), high proton conductivity (>100 mS cm^{-1}) is not an essential requirement for the ionomeric binder[27]. However, it is critical to prevent the formation of phosphonic acid anhydride to maintain the proton conductivity at a minimum level, about 0.1 mS cm^{-1}.

Phosphonated polymers have two benefits over ion-pair polymers for use as ionomeric binders. First, phosphonated polymers have immobilized phosphonic acid groups chemically bound to a polymer backbone, which results in no loss of acid functionality in the presence of water. Second, the low concentration of phosphonic acid (<4 milliequivalents per gram for phosphonated polymers versus 40 mequiv. g^{-1} for ion-pair polymers) mitigates the adverse

[1]Institute of Chemical Process Engineering, University of Stuttgart, Stuttgart, Germany. [2]MPA-11: Materials Synthesis and Integrated Devices, Los Alamos National Laboratory, Los Alamos, NM, USA. [3]Nanoscale Sciences Department, Sandia National Laboratories, Albuquerque, NM, USA. [4]Department of Chemical and Biological Engineering, Center for Micro-Engineered Materials (CMEM), University of New Mexico, Albuquerque, NM, USA. [5]T-1: Physics and Chemistry of Materials, Los Alamos National Laboratory, Los Alamos, NM, USA. [6]Chemical Resource Beneficiation, Faculty of Natural Sciences, North-West University, Potchefstroom, South Africa. [7]Forschungszentrum Jülich GmbH, Helmholtz Institute Erlangen-Nürnberg for Renewable Energy (IEK-11), Erlangen, Germany. [8]Present address: Materials Architecturing Research Center, Korea Institute of Science and Technology, Seoul, Republic of Korea. [9]These authors contributed equally: Vladimir Atanasov, Albert S. Lee. ✉e-mail: j.kerres@fz-juelich.de; yskim@lanl.gov

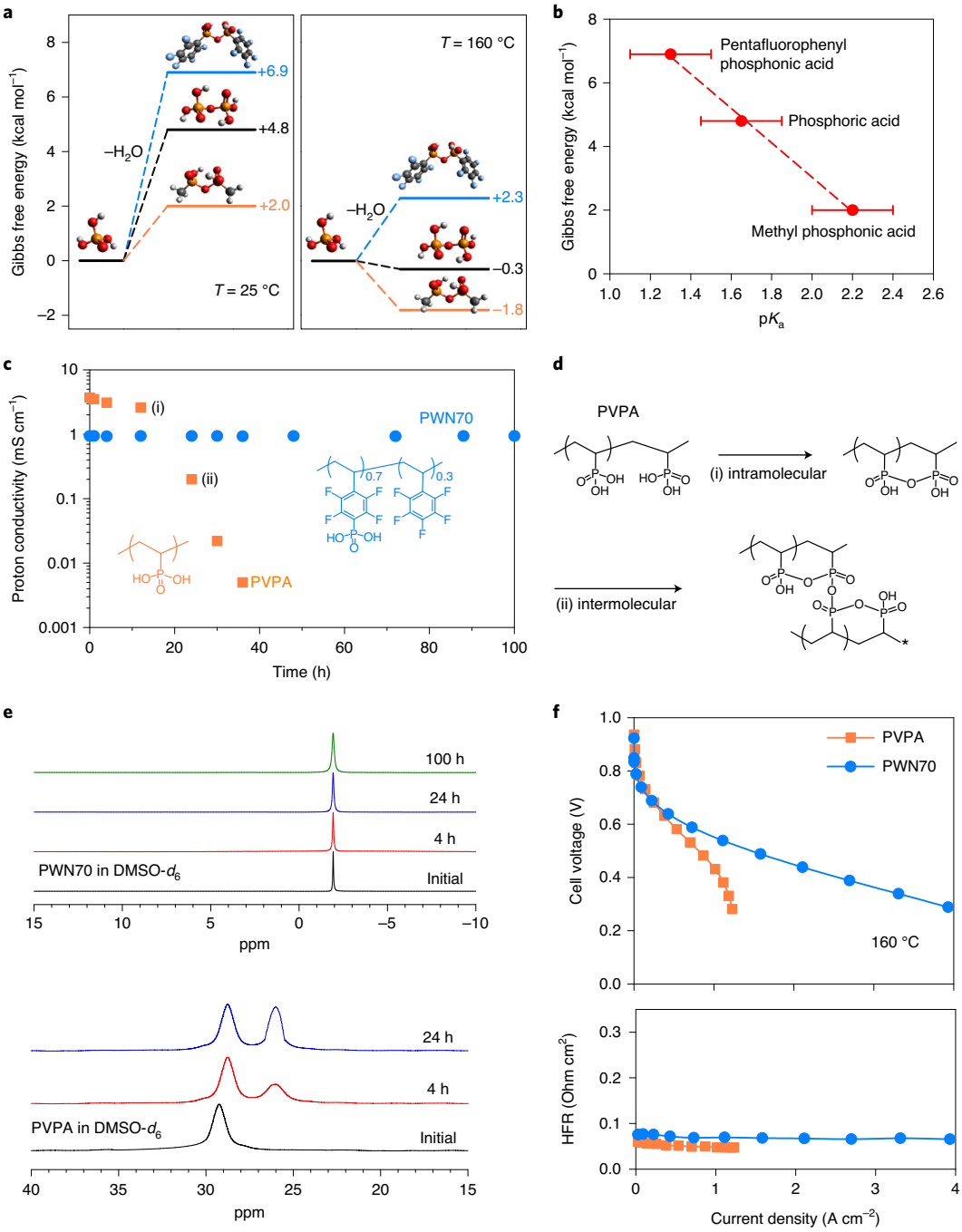

Fig. 1 | Anhydride formation of phosphonic acid. a, Gibbs free energy diagrams for the anhydride formation at 25 °C and 160 °C: phosphoric (black), methylphosphonic (orange) and pentafluorophenylphosphonic (light blue) acids. **b**, Correlation between the pK_a values of various phosphonic acids and the Gibbs free energy of phosphonic acid anhydride formation. The error bar of ±0.2 pK_a units was determined as a root-mean-square error in the fit of the experimental pK_a values to the DFT-calculated difference in the electronic energy of protonated and deprotonated forms of an acid. **c**, Anhydrous proton conductivity of 5 wt% PWN70 and PVPA solution in DMSO during 160 °C thermal treatment. The proton conductivity was measured at 80 °C. **d**, The formation of phosphonic acid anhydride of PVPA. (i) intermolecular polycondensation (pseudo-stable solution), (ii) intermolecular crosslinking (irreversible precipitation). **e**, Change in the ^{31}P NMR spectra of PWN70 (top) and PVPA (bottom), during 160 °C thermal treatment. **f**, H_2/O_2 fuel cell performance comparison between MEAs using PVPA and PWN70 ionomeric binder at 160 °C. Both MEAs used the same biphosphate-ammonium ion-pair membrane with same thickness. The performance was measured at H_2/O_2 (500/500 standard cubic centimetres per minute (sccm)) under P_{abs} = 147.1 kPa backpressure without humidification.

impact of phosphate poisoning at the cathode electrode and prevents electrode flooding by liquid phosphoric acid at the cathode.

Here, we introduce a fluorophenyl group to phosphonic acid to produce a phosphonated polymer that does not undergo undesirable phosphonic acid anhydride formation. We use the phosphonated polymer as an ionomeric binder in fuel cell electrodes in combination with an ion-pair coordinated membrane in a membrane electrode assembly (MEA) and evaluate their performance and

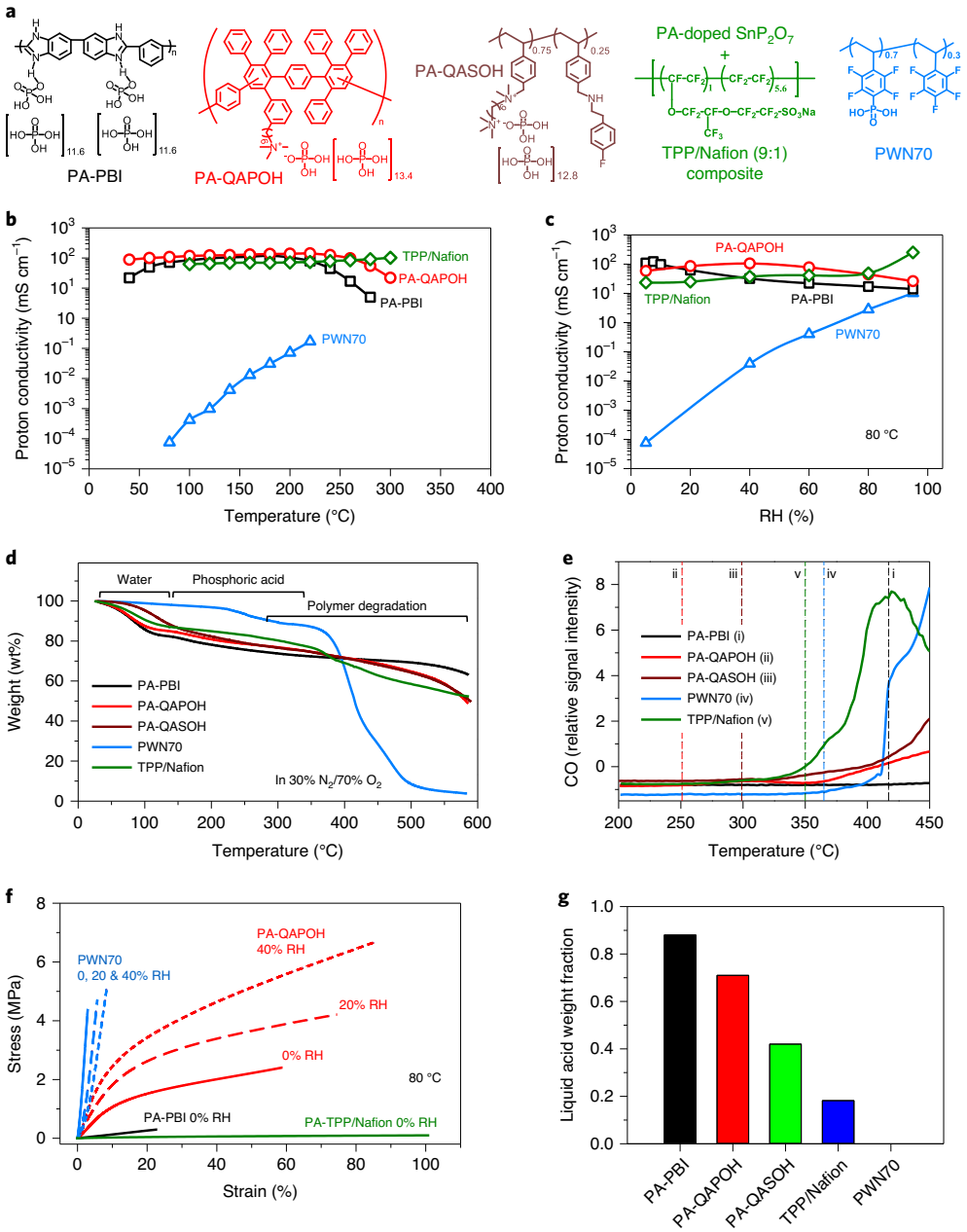

Fig. 2 | Property comparison of proton conductors. a, Chemical structure of proton conductors. **b**, Anhydrous proton conductivity of proton conductors as a function of temperature. The proton conductivity of PWN70 was obtained after drying the sample at 220 °C for 3 h. For the experimental procedure for other samples, see details in the Methods. The conductivity of QASOH could not be measured owing to the brittle nature of the film. **c**, Proton conductivity as a function of RH at 80 °C. The proton conductivity of PA-PBI and PA-QAPOH were taken from ref. [34]. **d**, TGA of proton conductors in 30 % N_2, 70 % O_2. **e**, CO relative intensity and thermal degradation temperature T_d determined by TGA–FTIR. **f**, Stress–strain curves as a function of RH at 80 °C. **g**, Liquid acid weight fraction of proton conductors.

durability by comparing with those of state-of-the-art HT-PEMFCs at the temperature range 120 to 240 °C.

Phosphonic acid anhydride formation

We hypothesized that the formation of acid anhydrides might not take place when the reactivity of the hydroxyl group in the phosphonic acid is low. To prove this, the thermodynamics of anhydride formation of phosphoric, methylphosphonic and pentafluorophenylphosphonic acids were examined by first-principles calculations using the MP2/6-31 G(d) level of theory[28] (Fig. 1a). At 25 °C, the Gibbs free energy for acid anhydride formation decreases in the order pentafluorophenylphosphonic acid (6.9 kcal mol^{-1}) > phosphoric acid (4.8 kcal mol^{-1}) > methylphosphonic acid (2.0 kcal mol^{-1}). These results indicate that the formation of the acid anhydrides is not a spontaneous process at room temperature due to the formation of high-energy P–O–P bonds[29]. However, at 160 °C the formation of acid anhydride becomes exergonic in the case of methylphosphonic acid (−1.8 kcal mol^{-1}) and slightly exergonic in the case of phosphoric acid (−0.3 kcal mol^{-1}). The anhydride formation of pentafluorophenylphosphonic acid becomes

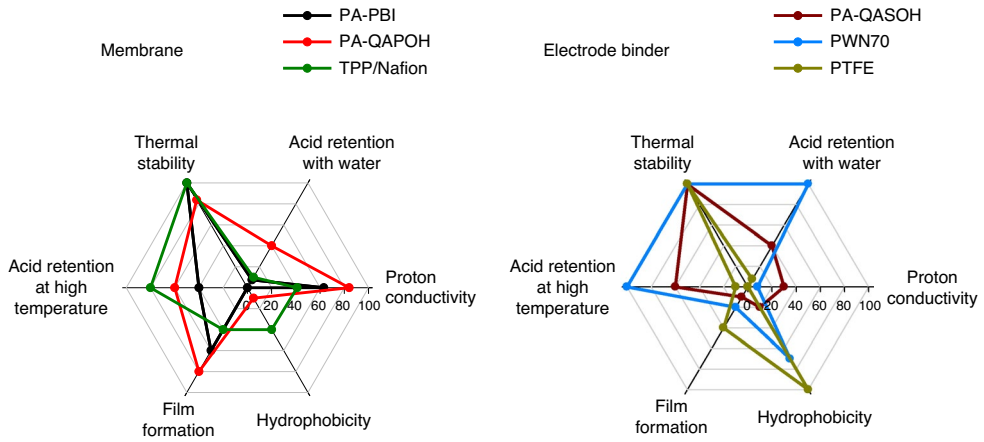

Fig. 3 | Property spider charts of materials to be used as membrane and electrode binder. The quantitatively defined criterion of each property is listed in the Methods.

exergonic at a higher temperature, about 240 °C (Extended Data Fig. 1). First-principles calculations show that the pentafluorophenylphosphonic acid anhydride is the least stable of all the studied anhydrides and therefore, the formation of the acid anhydride is endergonic even at 160 °C (2.3 kcal mol^{-1}). We also studied the protonation of methylphosphonic and pentafluorophenylphosphonic acids as one of the key steps towards the formation of anhydrides. The first-principles calculations show that the formation of the protonated pentafluorophenylphosphonic acid ($C_6F_5PO_3H_3^+$) is 5.6 kcal mol^{-1} more endergonic than the formation of the protonated methylphosphonic acid ($CH_3PO_3H_3^+$), which can be attributed to the difference in their acidity. Pentafluorophenylphosphonic acid has a smaller pK_a (where K_a is the acid dissociation constant) than the methylphosphonic acid, which makes protonation of this acid energetically more difficult. To verify the fact that increased dissociation of the proton suppresses phosphonic acid anhydride formation, we calculated the first pK_a of the acid compound analogues from a linear regression fit to experimental deprotonation energies[30]. The pK_a values of phosphoric, methylphosphonic and pentafluorophenylphosphonic acids at 25 °C are 1.65, 2.2 and 1.3, respectively, and correlate well with the anhydride formation Gibbs-free energy of the acid compounds (Fig. 1b). This result confirms that the high dissociation of hydroxyl proton stabilizes phosphonic acid, thus mitigating anhydride formation.

Next, a poly(2,3,5,6-tetrafluorostyrene-4-phosphonic acid) with a 70% degree of phosphonation (PWN70)[31], which has tetrafluorophenylphosphonic acid functional groups, was prepared and the proton conductivity of PWN70 was compared with that of poly(vinylphosphonic acid) (PVPA), which has methylphosphonic acid functional groups (Fig. 1c). The anhydrous solution proton conductivity of PWN70 was about 1 mS cm^{-1} and remained constant for 100 h after exposure of the polymer solution at 160 °C. The proton conductivity of PVPA was higher (4 mS cm^{-1}) at the beginning of the test, primarily owing to the higher concentration of protonic charge carriers in the polymer (4.6 versus 2.0 mequiv. g^{-1}). However, the conductivity of PVPA steadily decreased with time when the polymer solution was exposed to a temperature of 160 °C. During the first 40 h, the PVPA was soluble in dimethylsulfoxide (DMSO), suggesting intramolecular acid anhydride formation (i, Fig. 1d). After 40 h, the turbidity of the PVPA solution increased, indicating the start of intermolecular condensation (ii, Fig. 1d). The ^{31}P nuclear magnetic resonance (NMR) spectra of PWN70 showed only one ^{31}P NMR signal at −1.9 parts per million (ppm), which remained unchanged after the completion of the 100-h test (Fig. 1e). For the PVPA solution, only one phosphorus peak at 29.3 ppm appeared at the beginning of the test. However, another peak evolved over time at 26.0 ppm, corresponding to the phosphorus ether (P−O−P) originating from the formation of the phosphonic acid anhydride. We further investigated the possible acid anhydride formation of PWN70 at higher temperatures by ageing the polymer in the air at 200 °C and 240 °C. The proton conductivity of PWN70 remained stable at 200 °C (Extended Data Fig. 2a) for 100 h. The PWN70 polymer aged at 240 °C shows a reduced solubility in DMSO owing to phosphonic acid anhydride formation (Extended Data Fig. 2b). These results indicate that the strong electron-withdrawing fluorophenyl moiety of PWN70 provides electronic stabilization of the phosphonate anion.

We compared the fuel cell performance of MEAs using the PVPA and PWN70 ionomeric binders at 160 °C (Fig. 1f). The PWN70 MEA exhibited a substantially higher performance than the PVPA MEA. The similar high-frequency resistance values for both MEAs suggests that the difference in performance does not originate from the membrane. Electrochemical impedance analysis for the PWN70 and PVPA MEAs in the kinetic region, around 0.8 V, indicated that the charge transfer resistance of the PVPA MEA is 9.5 Ω cm^2, which is more than three times greater than that of the PWN70 MEA (2.8 Ω cm^2) (Extended Data Fig. 2c). This result suggests that the high proton transfer resistance of PVPA anhydride limits the performance of the MEA.

Property comparison for high-temperature polymer electrolytes

In this section, we compare the properties of state-of-the-art HT-PEMFC polymer electrolytes (Fig. 2a). First, we compared the anhydrous proton conductivity of the proton conductors as a function of temperature (Fig. 2b). The proton conductivity of PWN70 rapidly increased from 10^{-4} to 0.2 mS cm^{-1} as the temperature increased from 120 °C to 220 °C. The conductivity of PWN70 was slightly lower than that measured at 35% relative humidity (RH) (Extended Data Fig. 3). The proton conductivity of PA-PBI was at least three orders of magnitude higher than that of PWN70. The proton conductivity of PA-PBI increased with temperature and started to decrease at 190 °C, because of the evaporation of phosphoric acid. The proton conductivity of the ion-pair coordinated polymer (PA-QAPOH) was slightly higher than that of PA-PBI and kept increasing until a temperature of 220 °C was reached before decreasing. The maximum conductivity at the higher temperature for the ion-pair polymer may be due to the higher interaction of the

Table 1 | MEA components and fuel cell performance comparison

MEA name	Membrane	PEM thickness (μm)	Ionomeric binder	Anode catalyst (Pt loading)	Cathode catalyst (Pt loading)	Note and reference
MEA1	PA-PBI	50	PTFE	Pt/C (1.0 mg cm^{-2})	Pt-alloy/C (0.75 mg cm^{-2})	PA-PBI control[39]
MEA2	PA-PBI	50	PWN70	PtRu/C (0.5 mg cm^{-2})	Pt/C (0.6 mg cm^{-2})	This study
MEA3	PA-QAPOH	40	PA-QASOH			Ion-pair[3]
MEA4	PA-QAPOH	40	PWN70			This study
MEA5	PA-TPP/Nafion	80	PA-QASOH			Metal phosphate[40]

PEM, polymer electrolyte membrane

ion pair. The phosphoric-acid (PA)-doped tin pyrophosphate (TPP/Nafion) composite membrane exhibited slightly lower conductivity values than those of PA-PBI and PA-QAPOH in the temperature range 120–200 °C, with no decrease in conductivity up to 300 °C.

Acid retention in the presence of water was evaluated by measuring proton conductivity at 80 °C as a function of RH (Fig. 2c). The proton conductivity of PA-PBI showed the maximum value at 7.5% RH. At higher RH values, the proton conductivity of PA-PBI decreased, owing to the loss of phosphoric acid in the presence of water. The proton conductivity of PA-QAPOH showed the maximum value at 40% RH, indicating that the acid retention of PA-QAPOH is much higher. The conductivity of PWN70 kept increasing with RH because no acid loss occurred in the presence of water. TPP/Nafion has lower conductivity than PA-PBI and PA-QAPOH at low RH values, around <40% RH, but the conductivity increased at higher RH values owing to the contribution of Nafion.

The thermal oxidative stability of the proton conductors was compared in oxygen-enriched synthetic air (70% O_2, 30% N_2) by thermogravimetric analysis coupled to Fourier transform infrared spectroscopy (TGA–FTIR) (Fig. 2d). All samples exhibited a substantial mass loss below 300 °C. The weight loss of PA-PBI, PA-QAPOH, PA-QASOH and TPP/Nafion below 300 °C is relatively large, around 20%, owing to the evaporation of water and phosphoric acid. PA-PBI exhibits the highest thermal degradation temperature T_d, with the onset of CO evolution starting at 417 °C (Fig. 2e). The thermal degradation of PWN70 starts at 365 °C and progresses very quickly, losing most of the weight around 550 °C. The trace of weight loss at 220–350 °C may be due to the residual solvent and small anhydride formation at >220 °C (ref. [32]). Complete degradation of PWN70 and its precursor was examined with a continuous FTIR scanning of the evolved gases (Extended Data Fig. 4). The thermal degradation of TPP/Nafion took place at 350 °C, where Nafion starts to degrade[33]. Similar degradation profiles were observed for PA-QAPOH and PA-QASOH with T_d values of 251 °C and 299 °C, respectively. In both cases, the polymer degradation was very slow up to 360–400 °C, followed by acceleration of CO evolution above this temperature. The slow rate of degradation can be attributed to the de-alkylation of their quaternary ammonium side chains (Extended Data Fig. 5). The thermo-oxidative stability results indicated that the upper operating temperature of fuel cells would be limited by the evaporation of phosphoric acid (190–220 °C) before thermal degradation of the polymer (>250 °C) or anhydride acid formation of PWN70 (≥240 °C).

The mechanical properties of the proton conductors were evaluated at 80 °C (Fig. 2f). The tensile stress of PA-PBI at 0% RH was less than 0.29 MPa at about 20% strain. By contrast, the PA-QAPOH ion-pair membrane showed robust mechanical behaviour. The mechanical properties of the PA-QAPOH membrane increased with humidification. The elongation of the PA-QAPOH membrane increased due to the plasticization of the polymer by the absorbed water. The strength of the membrane also enhanced as the interaction energy of the ion-pair clusters in PA-QAPOH increased by the addition of water molecules[34]. The PWN70 membrane was found to be brittle owing to the strong hydrogen-bonding network of the phosphonic acid groups. The tensile strength of TPP/Nafion membrane was poor, whereas the elongation at the membrane break was high, owing to the high phosphate content in SnP_2O_7.

The liquid acid content of the proton conductors was measured by acid-base titration. Figure 2g shows that PA-PBI has the highest liquid acid fraction, followed by ion-pair polymers. TPP/Nafion has a relatively low phosphoric acid content. PWN70 has no liquid acid fraction as all phosphonic acid groups were covalently bound to the polymer.

Synergistic integration of polymer electrolytes in MEAs

Figure 3 shows spider charts of the six most critical parameters required to be a membrane or an electrode binder for candidate HT-PEMFCs. Whereas thermal stability, acid retention and anhydrous proton conductivity are required by both a membrane and electrode binder, film-formation ability is required only by the membrane, and hydrophobicity is required only by the electrode binder. For membrane candidates, the PA-QAPOH ion-pair membrane is superior to those of PA-PBI except for thermo-oxidative stability. The TPP/Nafion membrane has higher acid retention at high temperature, but its other properties were inferior to those of PA-PBI and PA-QAPOH, in particular, its film formation ability which is borderline acceptable. For ionomeric binder candidates, the PTFE binder has extremely high hydrophobicity to prevent electrode flooding. PWN70 has superior acid retention and hydrophobicity to those of PA-QASOH.

Fuel cell performance and durability

In this section, we compare the HT-PEMFC performance and durability of MEAs consisting of different combinations of membranes and electrode binders (Table 1). Figure 4a compares the fuel cell performance of the MEAs at 120 °C. For the PA-PBI MEAs, the PTFE binder (MEA1) exhibited a superior performance compared to that of the PWN70 binder (MEA2), consistent with previous findings that the PTFE binder performs well with a PA-PBI membrane[35,36]. MEA3 (ion-pair membrane/ionomer) and MEA5 (metal phosphate membrane/ion-pair ionomer) showed a performance similar to that of MEA2. The performance of MEA4 (ion-pair membrane/phosphonated ionomer) at low current density was comparable to that of MEA1 but had substantially better performance at high current density. At the operating temperature of 160 °C, the performance of MEA3 became superior to MEA1 (Fig. 4b). MEA4 exhibited improved high current density performance. As a result, the peak power density of MEA4 became about 1.5 times higher than that of the PA-PBI MEA (MEA1) (1,134 mW cm^{-2} for MEA4 versus 730 mW cm^{-2} for MEA1). The performance of MEA5 was low owing to relatively high high-frequency resistance. The impedance analysis at 0.2 V indicated that the gas diffusion resistance of

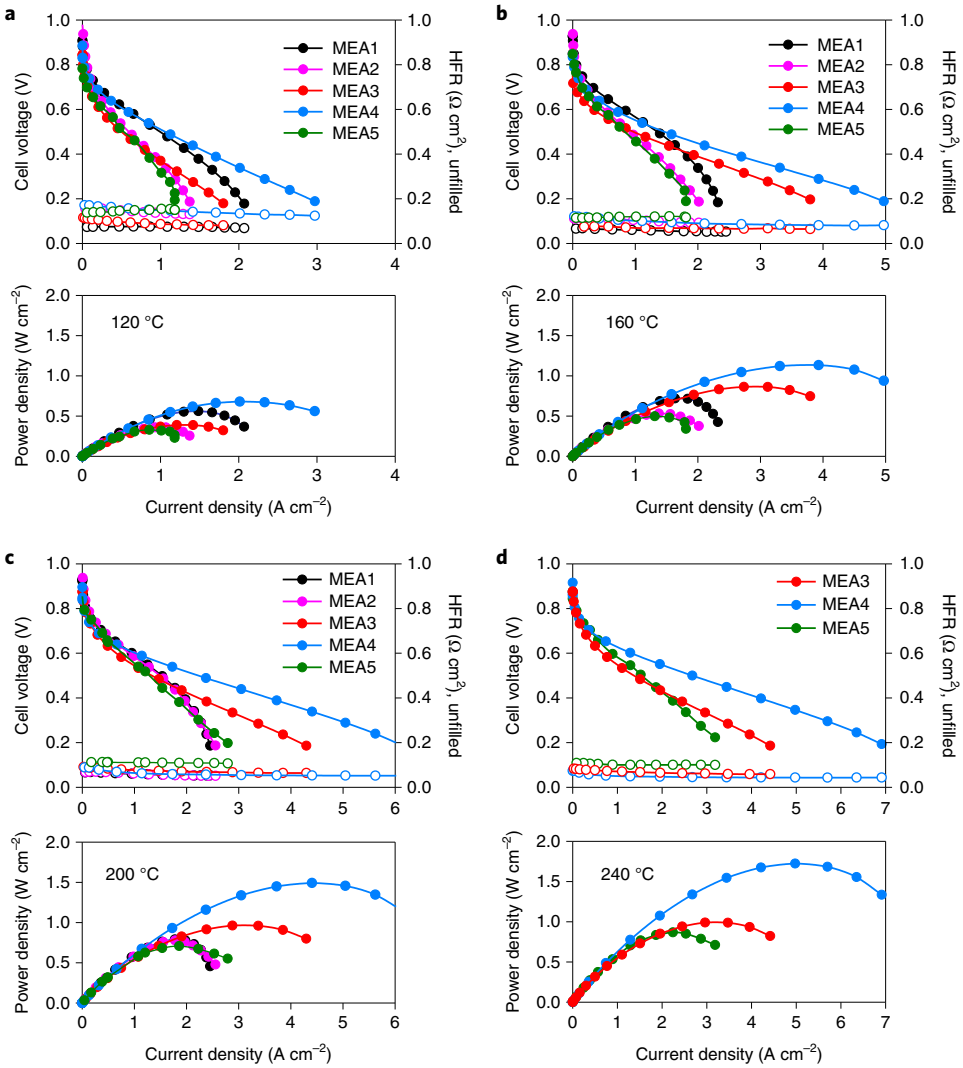

Fig. 4 | H_2/O_2 fuel cell performance comparison for different MEAs. HFR, high-frequency resistance. **a**, At 120 °C; **b**, at 160 °C; **c**, at 200 °C; and **d**, at 240 °C. The fuel cell performance was measured at H_2/O_2 (500/500 sccm) under 147.1 kPa absolute backpressure without humidification. At the operating temperature at 240 °C, the fuel cell performance of MEA1 and MEA2 degraded quickly, so we were unable to evaluate the performance accurately.

the PA-PBI MEA with the PTFE-bonded electrode (MEA1) was much higher (1.77 Ω cm²) than that of the ion-pair MEA with the phosphonated electrode (MEA4) (0.75 Ω cm²) (Extended Data Fig. 6). Furthermore, the gas diffusion resistance of the PWN70 electrode (MEA2 and MEA 4) did not increase much with the water vapour pressure, suggesting that the phosphonated ionomer can effectively handle additional water under higher-current-generating conditions. At the operating temperature of 200 °C, the difference in performance between the two best-performing MEAs (MEA4 and MEA3) became even greater (Fig. 4c). The peak power density of MEA4 reached 1,503 mW cm^{-2}, which was 1.5 times higher than that of MEA3 and 2.2 times higher than for a MEA based on a polycation-PBI blend membrane[37]. At the operating temperature of 240 °C, the peak power density of MEA4 reached 1,740 mW cm^{-2}, which was 1.7 to 2 times higher than those of MEA3 and MEA5 (Fig. 4d). The fuel cell performance of MEA5 was improved, but still lower than other MEAs because of the notably high ohmic resistance. The performance demonstrated here with MEA4 is substantially higher than that of the Nafion low-temperature (LT)-PEMFC using the same loading of Pt/C catalyst at 80 °C (Extended Data Fig. 7). The peak power density of MEA4 ranged from 309 mW cm^{-2} to 923 mW cm^{-2} at the operating temperature of 120–240 °C under H_2/air conditions, suggesting good mass transport at the PWN70 electrode (Extended Data Fig. 8).

The short-term durability of the MEAs under a constant cell current density of 0.15 A cm^{-2} was compared as a function of operating temperature (Fig. 5a–d). At 120 °C, the cell voltage of MEA1 slowly decreased (with decay rate 0.30 mV h^{-1}), accompanying a discernible increase in high-frequency resistance (0.48 mΩ cm² h^{-1}), suggesting that the performance loss is related to the loss of doped phosphoric acid in the MEA at 120 °C. Both MEA3 and MEA4 showed stable performance and high-frequency resistance. At 160 °C, all MEAs showed stable performance and high-frequency resistance over 100 h. At 200 °C, the cell voltage of MEA1 substantially decreased over time with a high decay rate (0.97 mV h^{-1}) and a large increase in cell high-frequency resistance (0.93 mΩ cm² h^{-1}). The performance of MEA3 also decreased (0.32 mV h^{-1}), accompanied by an increase in high-frequency resistance (0.28 mΩ cm² h^{-1}). At 240 °C, all tested MEAs were unstable. MEA1 and MEA2 degraded quickly and were unable to operate within 2 h. MEA3 and MEA5 could operate for about 18 h. MEA4 had a slightly longer lifetime (around 30 h). We observed increases

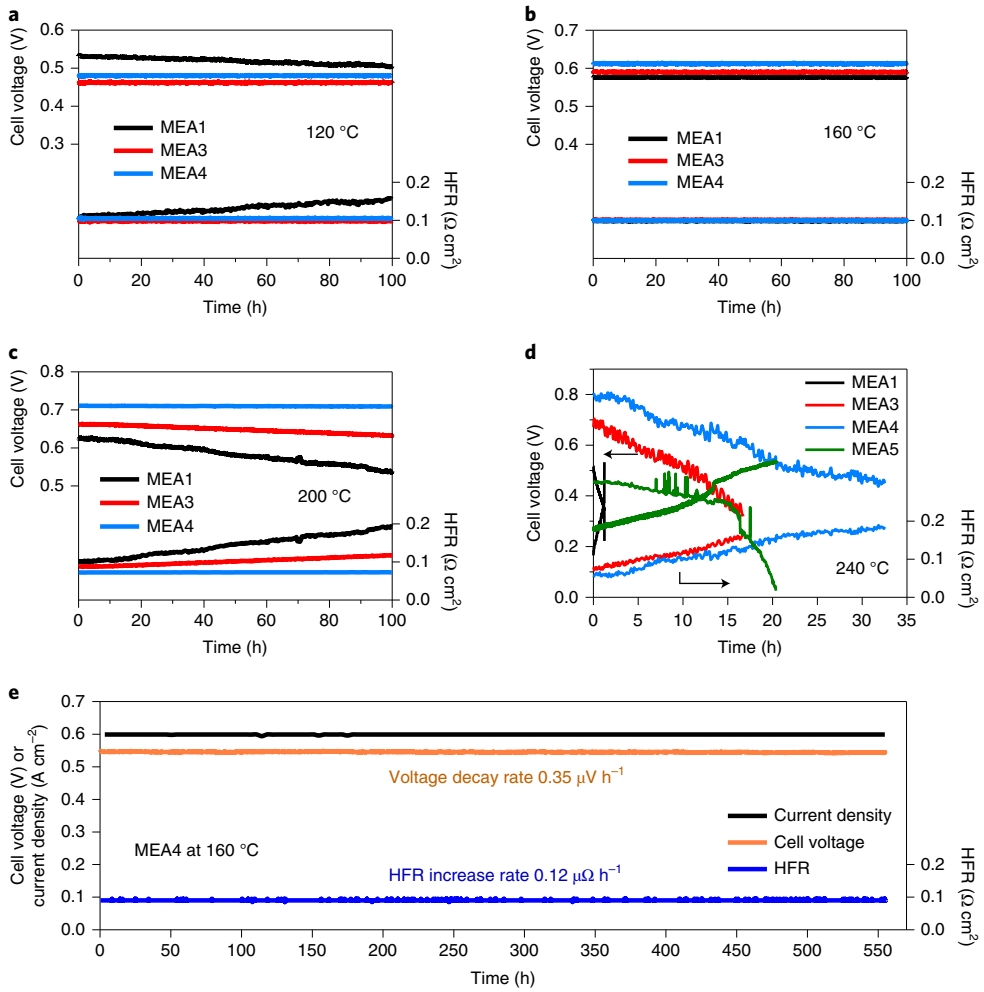

Fig. 5 | H_2/air fuel cell durability comparison for different MEAs. a, At 120 °C; **b**, at 160 °C; **c**, at 200 °C; and **d**, at 240 °C. Cell voltage was measured at H_2/air (500/500 sccm) under 147.1 kPa absolute backpressure and at a constant current density of 0.15 A cm^{-2}, without humidification. **e**, Durability of MEA4 at 160 °C at a constant current density of 0.6 A cm^{-2}.

in the values of high-frequency resistance for all MEAs during the extended-term test, suggesting that loss of phosphoric acid may be the primary cause of performance degradation. The slightly longer lifetime of MEA4 is probably due to the thermal stability of the ionomer. The results suggest that the hybrid MEA, consisting of the ion-pair membrane and PWN70 ionomer (MEA4), can extend both the low and high operating temperature limits from those of a conventional PA-PBI system (MEA1). The long-term durability of MEA4 at 160 °C was evaluated at a constant high current density of 0.6 A cm^{-2} (Fig. 5e). The cell performance was stable for >550 h until we stopped the test. The voltage decay was 0.35 μV h^{-1} and the rate of increase in high-frequency resistance was 0.12 μΩ h^{-1}. The much smaller loss of performance than what was observed in short-term testing suggest that most structural change occurs at the beginning of the test. We note the excellent electro-oxidative stability of the poly(pentafluorostyrene)-based ionomer of MEA4, which is probably due to a complexation of a metal cation such as Fe^{2+} with OH radicals from the H_2O_2 intermediate formed at the fuel cell electrodes[32,38].

In this study, we found that the phosphonated poly(pentafluorostyrene) (PWN70) did not undergo adverse anhydride formation at <240 °C and could be successfully integrated into a hybrid MEA with an ion-pair membrane. The PWN70 enables excellent fuel cell performance and durability over the temperature range of 120–200 °C that outperforms those of other state-of-the-art HT-PEMFC MEAs. The results indicate that properly designed phosphonated polymers can be used as an ionomeric binder for HT-PEMFCs. The ability to conduct protons without acid loss of this material design concept is desirable for other electrochemical applications that require electrochemical reaction at 120–240 °C. Stable operation at >200 °C remains a challenge.

Online content

Any methods, additional references, Nature Research reporting summaries, source data, extended data, supplementary information, acknowledgements, peer review information; details of author contributions and competing interests; and statements of data and code availability are available at https://doi.org/10.1038/s41563-020-00841-z.

Received: 19 March 2020; Accepted: 23 September 2020;
Published online: 07 December 2020

References

1. Choi, S. et al. Exceptional power density and stability at intermediate temperatures in protonic ceramic fuel cells. *Nat. Energy* **3**, 202–210 (2018).
2. Chandan, A. et al. High temperature (HT) polymer electrolyte membrane fuel cells (PEMFC)—a review. *J. Power Sources* **231**, 264–278 (2013).
3. Lee, K. S., Spendelow, J. S., Choe, Y. K., Fujimoto, C. & Kim, Y. S. An operationally flexible fuel cell based on quaternary ammonium-biphosphate ion pairs. *Nat. Energy* **1**, 16120 (2016).

4. Wilson, M. S. & Gottesfeld, S. Thin-film catalyst layers for polymer electrolyte fuel cell electrode. *J. Appl. Electrochem.* **22**, 1–7 (1992).
5. Wang, L. et al. An optimised synthesis of high performance radiation-grafted anion-exchange membranes. *Green Chem.* **19**, 831–843 (2017).
6. Huang, G. et al. Composite poly(norbornene) anion conducting membranes for achieveing durability, water management and high power (3.4 W/cm^2) in hydrogen/oxygen alkaline fuel cells. *J. Electrochem. Soc.* **166**, F637 (2019).
7. Li, D. et al. Highly quaternized polystyrene ionomers for high performance anion exchange membrane water electrolysers. *Nat. Energy* **5**, 378–385 (2020).
8. Liu, B. J. et al. Fluorinated poly(aryl ether) containing a 4-bromophenyl pendant group and its phosphonated derivative. *Macromol. Rapid. Comm.* **27**, 1411–1417 (2006).
9. Parvole, J. & Jannasch, P. Polysulfones grafted with poly(vinylphosphonic acid) for highly proton conducting fuel cell membranes in the hydrated and nominally dry state. *Macromolecules* **41**, 3893–3903 (2008).
10. Markova, D., Kumar, A., Klapper, M. & Mullen, K. Phosphonic acid-containing homo-, AB and BAB block copolymers via ATRP designed for fuel cell applications. *Polymer* **50**, 3411–3421 (2009).
11. Abu-Thabit, N. Y., Ali, S. A. & Zaidi, S. M. J. New highly phosphonated polysulfone membranes for PEM fuel cells. *J. Membr. Sci.* **360**, 26–33 (2010).
12. Atanasov, V. & Kerres, J. Highly phosphonated polypentafluorostyrene. *Macromolecules* **44**, 6416–6423 (2011).
13. Tamura, Y., Sheng, L., Nakazawa, S., Higashihara, T. & Ueda, M. Polymer electrolyte membranes based on polystyrenes with phosphonic acid via long alkyl side chains. *J. Polym. Sci. Pol. Chem.* **50**, 4334–4340 (2012).
14. Abouzari-Lotf, E., Ghassemi, H., Mehdipour-Ataei, S. & Shockravi, A. Phosphonated polyimides: enhancement of proton conductivity at high temperatures and low humidity. *J. Membr. Sci.* **516**, 74–82 (2016).
15. Sun, J. et al. Morphology and proton transport in humidified phosphonated peptoid block copolymers. *Macromolecules* **49**, 3083–3090 (2016).
16. Jang, S., Kim, S. Y., Jung, H. Y. & Park, M. J. Phosphonated polymers with fine-tuned ion clustering behavior: toward efficient proton conductors. *Macromolecules* **51**, 1120–1128 (2018).
17. Date, B. et al. Synthesis and morphology study of SEBS Triblock copolymers functionalized with sulfonate and phosphonate groups for proton exchange membrane fuel cells. *Macromolecules* **51**, 1020–1030 (2018).
18. Thompson, T. N. & Arnett, N. Y. Effect of phosphonated triazine monomer additive in disulfonated poly (arylene ether sulfone) composite membranes for proton exchange membrane fuel cells. *Polymer* **171**, 34–44 (2019).
19. Schuster, M., Kreuer, K.-D., Steininger, H. & Maier, J. Proton conductivity and diffusion study of molten phosphonic acid H_3PO_3. *Solid State Ion.* **179**, 523–528 (2008).
20. Schuster, M., Rager, T., Noda, A., Kreuer, K.-D. & Maier, J. About the choice of the protogenic group in PEM separator materials for intermediate temperature, low humidity operation: a critical comparison of sulfonic acid, phosphonic acid and imidazole functionalized model compounds. *Fuel Cells* **5**, 355–365 (2005).
21. Bingöl, B., Meyer, W. H., Wagner, M. & Wegner, G. Synthesis, microstruture, and acidity of poly(vinylphosphonic acid). *Macromol. Rapid Comm.* **27**, 1719–1724 (2006).
22. Rager, T., Schuster, M., Steininger, H. & Kreuer, K.-D. Poly(1,3-phenylene-5-phosphonic acid), a fully aromatic polyelectrolyte with high ion exchange capacity. *Adv. Mater.* **19**, 3317–3321 (2007).
23. Vilciauskas, L., de Araujo, C. C. & Kreuer, K.-D. Proton conductivity and diffusion in molten phosphinic acid (H_3PO_2): the last member of the phosphorus oxoacid proton conductor family. *Solid State Ion.* **212**, 6–9 (2012).
24. Melchior, J.-P., Majer, G. & Kreuer, K.-D. Why do proton conducting polybenzimidazole phosphoric acid membranes perform well in high-temperature PEM fuel cells? *Phys. Chem. Chem. Phys.* **19**, 601 (2017).
25. Wu, Q. & Weiss, R. A. Synthesis and characterization of poly (styrene-co-vinyl phosphonate) ionomers. *J. Polym. Sci. Pol. Phys.* **42**, 3628–3641 (2004).
26. Debe, M. K., Schmoeckel, A. K., Vernstrorn, G. D. & Atanasoski, R. High voltage stability of nanostructured thin film catalysts for PEM fuel cells. *J. Power Sources* **161**, 1002–1011 (2006).
27. Kim, Y. S. et al. Origin of toughness in dispersion-cast Nafion membranes. *Macromolecules* **48**, 2161–2172 (2015).
28. Frisch, M. J. et al. *Gaussian 09* Revision C.01 (Gaussian, Inc., 2010).
29. Hochstrasser, R. M. & King, D. S. Theoretical calculations of the hydrolysis energies of some "high energy" molecules. I. The phosphoric and carboxylic anhydrides. *J. Am. Chem. Soc.* **97**, 4762–4763 (1975).
30. Zhang, S., Baker, J. & Pulay, P. A reliable and efficient first principles-based method for predicting pK_a values. 2. Organic acids. *J. Phys. Chem. A* **114**, 432–442 (2010).
31. Atanasov, V., Oleynikov, A., Xia, J. B., Lyonnard, S. & Kerres, J. Phosphonic acid functionalized poly(pentafluorostyrene) as polyelectrolyte membrane for fuel cell application. *J. Power Sources* **343**, 364–372 (2017).
32. Atanasov, V., Gudat, D., Ruffmann, B. & Kerres, J. Highly phosphonated polypentafluorostyrene: characterization and blends with polybenzimidazole. *Eur. Polym. J.* **49**, 3977–3985 (2013).
33. Wilkie, C. A., Thomsen, J. R. & Mittleman, M. L. Interaction of poly (methyl-methacrylate) and Nafions. *J. Appl. Polym. Sci.* **42**, 901–909 (1991).
34. Lee, A. S., Choe, Y. K., Matanovic, I. & Kim, Y. S. The energetics of phosphoric acid interactions reveals a new acid loss mechanism. *J. Mater. Chem. A* **7**, 9867–9876 (2019).
35. Park, J. O. et al. Role of binders in high temperature PEMFC electrode. *J. Electrochem. Soc.* **158**, B675–B681 (2011).
36. Su, H. N., Pasupathi, S., Bladergroen, B., Linkov, V. & Pollet, B. G. Optimization of gas diffusion electrode for polybenzimidazole-based high temperature proton exchange membrane fuel cell: evaluation of polymer binders in catalyst layer. *Int. J. Hydrogen Energy* **38**, 11370–11378 (2013).
37. Venugopalan, G. et al. Stable and highly conductive polycation-polybenimidazole membrane blends for intermediate temperature polymer electrolyte membrane fuel cells. *ACS Appl. Energy Mater.* **3**, 573–585 (2020).
38. Kerres, J. & Atanasov, V. Cross-linked PBI-based high temperature membranes: stability, conductivity and fuel cell performance. *Int. J. Hydrogen Energy* **40**, 14723–14735 (2015).
39. De Castro, E. PBI-phosphoric acid based membrane electrode assemblies: status update. In *MCFC and PAFC R&D Workshop Summary Report.* https://www1.eere.energy.gov/hydrogenandfuelcells/pdfs/mcfc_pafc_workshop_summary.pdf (US Department of Energy, 2010).
40. Lee, K. S. et al. Intermediate temperature fuel cells via an ion-pair coordinated polymer electrolyte. *Energy Environ. Sci.* **11**, 979–987 (2018).

Publisher's note Springer Nature remains neutral with regard to jurisdictional claims in published maps and institutional affiliations.

© Triad National Security under exclusive licence to Springer Nature Ltd 2020

Methods

Materials. All chemicals and solvents were purchased from Sigma-Aldrich unless specifically indicated. Commercial 60 wt% Pt/C (HiSPEC 9100) and 50% PtRu/C (Pt:Ru 2:1, HiSPEC 12100) catalysts were purchased from Johnson Matthey for the cathode and anode, respectively. PVPA was purchased from Sigma Aldrich in powder form and used as received. Single-sided ELAT gas diffusion layers were purchased from E-TEK. Commercial PBI membranes were purchased from Celazole. Commercial PA-PBI MEAs were kindly provided by Advent.

Synthesis of QAPOH. QAPOH was prepared as described by Hibbs[41]. First, brominated alkyl ketone functionalized Diels–Alder poly(phenylene) was synthesized by reacting Diels–Alder poly(phenylene) with 6-bromohexanoyl chloride in the presence of aluminum chloride. The ketone groups of the polymer were reduced to methylene groups by a reaction with trifluoroacetic acid and triethylsilane. The membrane was aminated by immersion in trimethylamine solution (45% w/w in water) for 48 h. For the non-aqueous process, bromoalkylated Diels–Alder poly(phenylene)[42] was dissolved in *N*-methyl-2-pyrrolidone at a concentration of 5% by weight, followed by adding excess trimethylamine (10 equivalents of amine to alkyl bromide) in anhydrous ethyl alcohol dropwise to prevent the polymer from precipitating from solution. The solution was heated to 40 °C for 48 h and then quenched by pouring the solution into a 10% solution by weight of acetic acid. The polymer was then rinsed with deionized water until the pH was neutral and dried in a vacuum oven at 50 °C overnight.

Synthesis of SnP_2O_7 particles. The SnP_2O_7 particles were prepared as described in our previous paper[40]. 6.2 g of $SnCl_4$ hydrate was dissolved in 30 g of alcohol, to which 10.1 g of diammonium phosphate dissolved in 12.2 g of hot water was quickly added with vigorous stirring. The mixture was heated and evaporated with continued stirring until thickening, then removed from heat. Cooling resulted in a thick 'frosting' that was dried at 60 °C. The foamy mass was fired in a covered crucible at 650 °C for 2.5 hours. The product was dry-milled with zirconia balls to form a fine powder.

Synthesis of QASOH. Poly(vinylbenzyl chloride) (500 mg) was dissolved in dimethyl sulfoxide (10 ml) in a 40 ml vial, and 6-(dimethylamino)-*N,N,N*-trimethyl-1-hexanaminium iodide (258 mg, synthesized from *N,N,N′,N′*-tetramethyl-1,6-hexanediamine and methyl iodide in tetrahydrofuran) was added to the solution. After stirring at 80 °C for 3 h, 4-fluorophenylamine (377 mg) was added, and the solution was stirred for 12 h at 80 °C. The solution was precipitated in diethyl ether and washed thoroughly to isolate the product as a light yellow powder. ^{1}H NMR spectrum of QASOH is shown in (Extended Data Fig. 9a). The powder was treated with 1 M NaOH solution to exchange counter-ions into the hydroxide form, washed thoroughly with deionized water and dried under vacuum. QASOH (the OH^- form) was then dissolved in the mixture of ethanol and isopropanol (1:1 v/v) to produce the 5 wt% ionomeric binder solution.

Synthesis of the phosphonated polymer PWN70. The degree of phosphonation of the PWN polymer was determined based on the properties of PWNs. PWNs have a reasonably high conductivity with <80% water uptake.[31] PWN70 was synthesized following a literature report[31]. Briefly, polypentafluorostyrene (100 g, 515 mmol monomer units, molecular weight $M_w = 200$ kDA, polydispersity index (PDI) = 3.4) was dispersed in *N,N*-dimethylacetamide (400 ml) and tris(trimethylsilyl)phosphite (200 g, 670 mmol) was added slowly. The reaction solution was then heated to 160 °C and magnetically stirred overnight. After the reaction was completed, the warm mixture was precipitated in 2 litres of water and collected via filtration. The resulting white powder was refluxed in water three times for 30 min each, exchanging water each time, followed by boiling in a 2 wt% phosphoric acid solution. Washing with water until neutral and drying at 140 °C yielded the phosphonated polymer with a 70% degree of phosphonation, PWN70. Yield 130 g (99%). The chemical structure and the molecular weight of PWN70 were analysed by ^{19}F NMR and gel permeation chromatography, respectively (Extended Data Fig. 9b, c).

SnP_2O_7/Nafion composite PEM fabrication. The Nafion membrane was dispersed in 1,2-pentanediol at 140 °C for 2 h after converting precleaned Nafion212 (Ion Power) to sodium form using 2% NaOH solution for 1.5 h and subsequent rinsing with deionized water for 1 h (ref. [27]). The prepared SnP_2O_7 particles were mixed to this Nafion dispersion. The SnP_2O_7/Nafion mixture was cast onto a clean glass plate at 120 °C for 3 h, dried under vacuum at 160 °C for 4 h, and finally heat-treated at 190 °C for an additional 4 h under ambient pressure. The composite membrane was doped with phosphoric acid by immersing the membrane into 85% phosphoric acid for 3 h at room temperature.

General membrane doping procedure. In a glass bath, pre-cut membranes were completely submerged in 85 wt% phosphoric acid solution overnight at room temperature. After blotting away excess phosphoric acid on the surface of the membrane, the doped membrane was stored in a convection oven set at 80 °C to dehydrate the membrane for at least 2 h prior to fuel cell testing. Phosphoric acid doping levels were calculated using our previous method[3].

Acid content measurement. The ion-exchange capacity (IEC) of PWN70 was determined by titration. The sample was immersed in a saturated sodium chloride solution for 24 h followed by a titration with 0.1 M NaOH to the equivalent point. Then a defined excess of NaOH was added, stirred for 24 h and the solution was back-titrated with 0.1 M HCl. The doping level of PA-PBI, PA-QAPOH and PA-QASOH were determined by acid-base titration through the following procedure: (i) dry membrane samples were weighed; (ii) the samples were titrated with 0.1 M NaOH solution using phenolphthalein as an indicator; and (iii) the samples were washed with water and dried in a vacuum plate at 100 °C for 3 h and weighted again. The number of phosphoric acid molecules per repeat unit (X) was calculated from the following equation:

$$X = \frac{V_{\mathrm{NaOH}} C_{\mathrm{NaOH}}}{\left(\mathrm{MolEquiv}\left(\frac{w_{\mathrm{dry}}}{M_{\mathrm{W}}}\right)\right)} \quad (1)$$

where V_{NaOH} (in litres) is the volume of NaOH, C_{NaOH} (in moles per litre) is the molar concentration of NaOH and MolEquiv is the equivalent number of moles of titrant for phosphoric acid, which is 3; three moles of NaOH reacts with one mole of phosphoric acid to produce trisodium phosphate.

The acid content of the membrane was determined gravimetrically. First, the undoped membrane was weighed and the weight was recorded as dry weight. Second, the phosphoric acid doped sample was weighed after drying at 80 °C for 24 hours (wet weight). The weight fraction of phosphoric acid (x) was calculated from the following equation.

$$x = \frac{(\text{wet weight minus dry weight})}{\text{wet weight}} \quad (2)$$

First principles calculations. Electronic structure calculations for the study of anhydride formation were performed using the MP2/6-31 G(d)[43–47] level of theory as implemented in the Gaussian09 quantum chemistry program (revision C.01)[28]. In all cases the structure of acids and anhydrides were optimized and the change in the reaction Gibbs free energy was calculated at 25 °C, 160 °C and 240 °C by performing the frequency analysis at the corresponding temperatures.

The pK_a values were calculated from a linear regression fit to experimental deprotonation energies using the equation $pK_a = a\left(E_A^- - E_{HA}\right) + b$; where E_A^- denotes the density functional theory (DFT)-calculated electronic energy of the deprotonated acid and E_{HA} denotes the DFT-calculated energy of the protonated acid. This approach was extensively tested in ref. [48] In this case, we derived a and b values using a dataset of nine experimental pK_a values: phenyl phosphonic acid (pK_a = 1.83), 2-fluoro-phenyl phosphonic acid (pK_a =1.64), 3-chloro-phenyl phosphonic acid (pK_a = 1.53), phosphoric acid (pK_a = 1.90), methyl phosphonic acid (pK_a = 2.35), dichloromethyl phosphonic acid, (pK_a = 1.14), chloromethyl phosphonic acid (pK_a = 1.51), etidronic acid (pK_a = 1.35) and phenyl dihydrogen phosphate (pK_a = 1.46). A full geometry optimization of both undissociated and dissociated acids were performed using the SMD solvation model[49] with water as solvent. For the calculation of pK values, the M06-2X/6-311++G(d,p)[50] level of theory and the Gaussian09 program (revision C.01) was used. Linear fitting of the experimental pK_a values to DFT calculated $\Delta E = \left(E_A^- - E_{HA}\right)$ values results in the equation of line pK_a = 0.108 * $(E_A^- - E_{HA})$ − 28.2; with R^2 of 0.90 and root-mean-square error of 0.2 pK_a units. The ΔE for pentafluorophenyl phosphonic acid was calculated as 273.34 kcal mol^{-1} and therefore its pK_a was determined to be 1.3 ± 0.2.

Thermal oxidative stability. Thermal oxidative stability of the proton conductors was measured by TGA–FTIR (STA 449 F3 Jupiter ASC with Perseus-Coupling System from Netzsch). The temperature scan was performed from 30 °C to 600 °C at a heating rate of 5 °C min^{-1} in synthetic oxygen-enriched air (O_2 70%; N_2 30%). The thermal degradation temperatures (T_d) of the proton conductor were defined as onset temperatures at which the first CO evolution in the corresponding temperature in the FTIR spectrum was observed.

Mechanical property measurements. The mechanical properties were conducted on a TA Q800-RH DMA instrument. Film samples of dimension 1 cm × 4 cm × 30 μm were used. For humidity-controlled experiments, the temperature of the environmental chamber was increased to 80 °C at 2 °C min^{-1}. After equilibrating the samples at a given RH for 1 h, the tensile measurement was performed at a load-ramp of 0.5 MPa min^{-1}. For the PA-PBI membrane, we measured the mechanical properties only at 0% RH since the mechanical properties change at higher RH as the phosphoric acid is lost. For the PA-QAPOH ion-pair membrane and PWN70, the mechanical properties were measured up to 40% RH.

Conductivity measurements. The conductivity of polymer electrolytes was measured either in a solution or with a stand-alone membrane. For the phosphonic acid anhydride formation study, the conductivity of PWN70 and PVPA was compared in solution form using a solution conductivity cell, owing to the brittle nature of the PVPA anhydride[46]. The cell used for liquid conductivity was

custom-made with stainless steel electrodes (electrode diameter 1 cm), that were 1 cm apart, encased in polypropylene casing (Extended Data Fig. 10a). For the anhydride formation study, a 5 wt% solution of both PWN70 and PVPA in a 1:1 mixture of anhydrous DMSO: DMSO-d_6 was heat-treated at 160 °C. Aliquots from this solution (about 5 ml) were taken for measurements of conductivity and ^{31}P NMR at various time intervals. The solution was filled with the solution conductivity cell and the whole solution conductivity cell was placed in a convection oven at 80 °C. After reaching the thermal equilibrium (about 1 h), the solution conductivity was measured by a National Instruments 1260 A Impedance/Gain-Phase Analyzer over a frequency range of 1 Hz to 1 MHz. For the anhydride formation study at higher temperatures of about 200 °C and 240 °C, we aged the PWN70 at the given temperature up to 100 h. The aged PWN 70 samples were dissolved in DMSO (5 wt%), and the conductivity was measured using the solution conductivity cell and the same procedure.

For in-plane film conductivity measurement, we used window cells with two different dimensions (Extended Data Fig. 10b, c). For the polymer membrane with high conductivity (> 10 mS cm^{-1}), we used a large window cell (width of the window 2 cm). For the polymer membrane with low conductivity (PWN70), we used a small window cell (width of the window 0.5 cm). For the large window cell, samples dimensions were 1 cm × 4 cm × 30 μm and custom-built PTFE blocks used to clamp the samples in place with stainless steel electrodes (2 cm apart), as described previously[47]. For temperatures 80 °C and with and without humidity, a humidity-controlled oven was used to control temperature and humidity and at least 12 h equilibrium time was given prior to measurement. For anhydrous measurements between the temperatures of 100 °C to 280 °C, a convection oven was used as the chamber. For temperatures 300 °C and above, the insulating PTFE blocks were substituted with commercial glass fibre filter paper (Whatman GF/A) without binder, which has a thickness of 0.26 mm and upper operating temperature of 550 °C, and the connecting metal cables were stripped of insulating materials and inserted in a Thermo Scientific tube furnace (Lindberg/Blue M) as the temperature control chamber. For the small window cell, sample dimensions were 1 cm × 2 cm × 100 μm. To prevent premature failure of the PWN70 membrane during the dehydration, we pre-dried the PWN70 membrane at 60 °C overnight. To reduce the electrode contact resistance, we clamped the PWN70 membrane with 1 mm between the stainless steel electrodes. The whole window cell was placed in a convection oven at 160 °C for 20 min to dry further; then the conductivity of the membrane was measured on heating and cooling at 20 °C intervals between 80 °C and 220 °C. Instrumentation as above was used for the membrane conductivity measurements. We also measured the conductivity of the polymer membranes as a function of RH at 80 °C. For this measurement, the window cell fixture was placed in a temperature/humidity controlled oven. The RH changed from 95% to 5%. The conductivity was measured after reaching the RH equilibrium state (1 h) at the given RH.

Spider chart. The spider chart was generated for six properties: (i) proton conductivity at 160 °C, (ii) acid retention with water, (iii) thermo-oxidative stability, (iv) acid evaporation temperature, (v) film formability and (vi) hydrophobicity. The criterion of each property was scaled to 100. Below are the criteria and scaling for each property:

i. Proton conductivity at 160 °C: 1,000 mS cm^{-1} (the highest conductivity from the compared proton conductors). The scale for the proton conductivity is logarithmic: 1,000 mS cm^{-1} (100), 100 mS cm^{-1} (80), 10 mS cm^{-1} (60), 1 mS cm^{-1} (40), 0.1 mS cm^{-1} (20) and 0.01 mS cm^{-1} (0).
ii. Acid retention in the presence of water: %RH with the maximum conductivity at 80 °C.
iii. Thermo-oxidative stability: 300 °C (the upper limit of operating temperature).
iv. Acid evaporation temperature: 260 °C or higher (100); 240 °C (80); 220 °C (60); 200 °C (40), 180 °C (20) and 160 °C (10).
v. Film formability in the dry state: solid film with tensile strength >20 MPa and elongation >30% (100); plasticized film with tensile strength > 2 MPa and elongation >30% (80), gel film with tensile strength >0.1 MPa and elongation >20% (60), fragile film with tensile strength > 0.01 MPa and elongation >20% (40), castable film with tensile strength > 0.01 MPa and elongation >2% (20), and the powder form (10).
vi. Hydrophobicity: Teflon-like (100), Nafion-like (80), fluorinated hydrocarbon (60), liquid content <0.2 (40), liquid content <0.5 (20), liquid content <0.8 (10).

Electrode preparation. Catalyst inks were composed of 60 wt% Pt/C or 50 wt% PtRu/C, PWN70 5 wt% dispersion in *N*,*N*-dimethylacetamide or PA-QASOH 5 wt% in ethanol, water and isopropyl alcohol, respectively. The ink compositions were 1.5 wt% of 60 wt% Pt/C catalyst, 3.5 wt% ionomer solution, 22 wt% deionized water and 77 wt% of isopropanol. The inks were sonicated via tip sonicator for 90 seconds prior to brush painting on pre-cut 5 cm^2 E-TEK carbon cloth gas diffusion layers set on a vacuum hot plate set at 80 °C. For the PA-QASOH ionomer electrodes, two small drops of 85 wt% phosphoric acid were dropped on top of the gas diffusion electrodes for 10 min and any excess phosphoric acid was blotted away immediately prior to fuel cell testing. Catalyst loadings (cathode: 0.6 mg of Pt per cm^2; anode: 0.5 mg of Pt per cm^2) were confirmed with X-ray fluorescence spectroscopy. Single cells were fabricated with serpentine graphite flow fields, Furon gaskets, and 5 cm^2 active area gas diffusion electrodes sandwiched between the phosphoric acid-doped membranes.

Fuel cell testing and impedance analysis. The H_2/O_2 fuel cell performance of the MEAs was measured using a fuel cell test station (Fuel Cell Technologies). MEA1 and MEA2 which use PA-PBI PEMs, were first heated to 120 °C under anhydrous N_2 flow, at which point gases were switched to H_2 and O_2 and cell temperature was further increased to 160 °C. The current increase was monitored at constant voltage of 0.6 V until stabilization (12 h). For MEA3, MEA4 and MEA5, current increase was monitored at a constant voltage of 0.6 V as cell temperature was raised from room temperature to 160 °C. After stabilization at 160 °C for 4 h, the cell voltage was lowered to 0.5 V, at which the current density increased further. An additional stabilization time of >10 h was required for full activation. Polarization curves and high-frequency resistance values for the MEAs were obtained at cell temperatures of 160 °C and 240 °C. H_2 and O_2 were supplied at 500 sccm without humidification and 147.1 kPa absolute backpressure applied to both anode and cathode. Electrochemical impedance analysis experiments were carried out with a Biologic SP-200 potentiostat at 0.2 V with a frequency range of 100 mHz to 1 MHz. H_2 and air were supplied at 500 sccm either without humidification or 19 kPa of water vapour pressure. The absolute backpressure of 147.1 kPa was applied to both anode and cathode. The impedance spectra were obtained at 0.8 V (kinetic region) and 0.2 V (mass transport region) at a frequency range of 0.1 Hz to 1 MHz.

Data availability

All the data represented in Figs. 1–5 and Extended Data Figs. 2–9 are provided with the paper as source data. All other data that support results in this Article are available from the corresponding author upon reasonable request. Source data are provided with this paper.

References

41. Hibbs, M. R. Alkaline stability of poly(phenylene)-based anion exchange membranes with various cations. *J. Polym. Sci. B* **51**, 1736–1742 (2013).
42. Park, E. J. et al. Alkaline stability of quaternized Diels-Alder polyphenylenes. *Macromolecules* **52**, 5419–5428 (2019).
43. Frisch, M. J., Head-Gordon, M. & Pople, J. A. Direct MP2 gradient method. *Chem. Phys. Lett.* **166**, 275–280 (1990).
44. Frisch, M. J., Head-Gordon, M. & Pople, J. A. Semi-direct algorithms for the MP2 energy and gradient. *Chem. Phys. Lett.* **166**, 281–289 (1990).
45. Head-Gordon, M., Pople, J. A. & Frisch, M. J. MP2 energy evaluation by direct methods. *Chem. Phys. Lett.* **153**, 503–506 (1988).
46. Saebø, S. & Almlöf, J. Avoiding the integral storage bottleneck in LCAO calculations of electron correlation. *Chem. Phys. Lett.* **154**, 83–89 (1989).
47. Head-Gordon, M. & Head-Gordon, T. Analytic MP2 frequencies without fifth order storage: theory and application to bifurcated hydrogen bonds in the water hexamer. *Chem. Phys. Lett.* **220**, 122–128 (1994).
48. Zhang, S. M., Baker, J. & Pulay, P. A reliable and efficient first principles-based method for predicting pK_a values. 1. Methodology. *J. Phys. Chem. A* **114**, 425–431 (2010).
49. Marenich, A. V., Cramer, C. J. & Truhlar, D. G. Universal solvation model based on solute electron density and on a continuum model of the solvent defined by the bulk dielectric constant and atomic surface tensions. *J. Phys. Chem. B* **113**, 6378–6396 (2009).
50. Zhao, Y. & Truhlar, D. G. The M06 suite of density functionals for main group thermochemistry, thermochemical kinetics, noncovalent interactions, excited states, and transition elements: two new functionals and systematic testing of four M06-class functionals and 12 other functionals. *Theor. Chem. Acc.* **120**, 215–241 (2008).

Acknowledgements

This work was supported by the US Department of Energy, Energy Efficiency and Renewable Energy, Hydrogen and Fuel Cell Technologies Office (HFTO) and the Advanced Research Project Agency-Energy (ARPA-E). This work was also partly supported from the Bundesministerium für Bildung und Forschung (BMBF) on account of the 'HT-Linked' project with Förderkennzeichen: 03SF0531C. Los Alamos National Laboratory is operated by Triad National Security, LLC under US Department of Energy contract number 89233218CNA000001. Sandia National Laboratories is a multi-programme laboratory operated by Sandia Corporation, a wholly owned subsidiary of Lockheed Martin Company, for the US Department of Energy's National Nuclear Security Administration under contract DE-AC04-94AL85000. I.M. acknowledges the computational resources from the Tri-Lab computing resources of Los Alamos National Laboratory and University of New Mexico Center for Advanced Research Computing. We thank E. De Castro and C. Kreller for providing the commercial PA-PBI MEA and SnP_2O_7, respectively. We also thank A. Muenchinger and K.-D. Kreuer for providing PWN70 conductivity data and discussions. This paper describes objective technical results and analysis. Any subjective views or opinions

that might be expressed in the paper do not necessarily represent the views of the US Department of Energy of the United States Government.

Author contributions

Y.S.K. designed and directed the study. V.A. and J.K. prepared the phosphonated polymers. A.S.L. performed electrochemical measurements. E.J.P., E.D.B., C.F. and M.H. prepared the ion-pair polymers. A.S.L., V.A., E.J.P., S.M., E.D.B., C.F., M.H. and Y.S.K. characterized polymers. I.M. performed the first principles calculations. A.S.L. and Y.S.K. wrote the paper, with contributions from all co-authors.

Competing interests

The authors declare no competing interests.

Additional information

Extended data is available for this paper at https://doi.org/10.1038/s41563-020-00841-z.

Correspondence and requests for materials should be addressed to J.K. or Y.S.K.

Reprints and permissions information is available at www.nature.com/reprints.

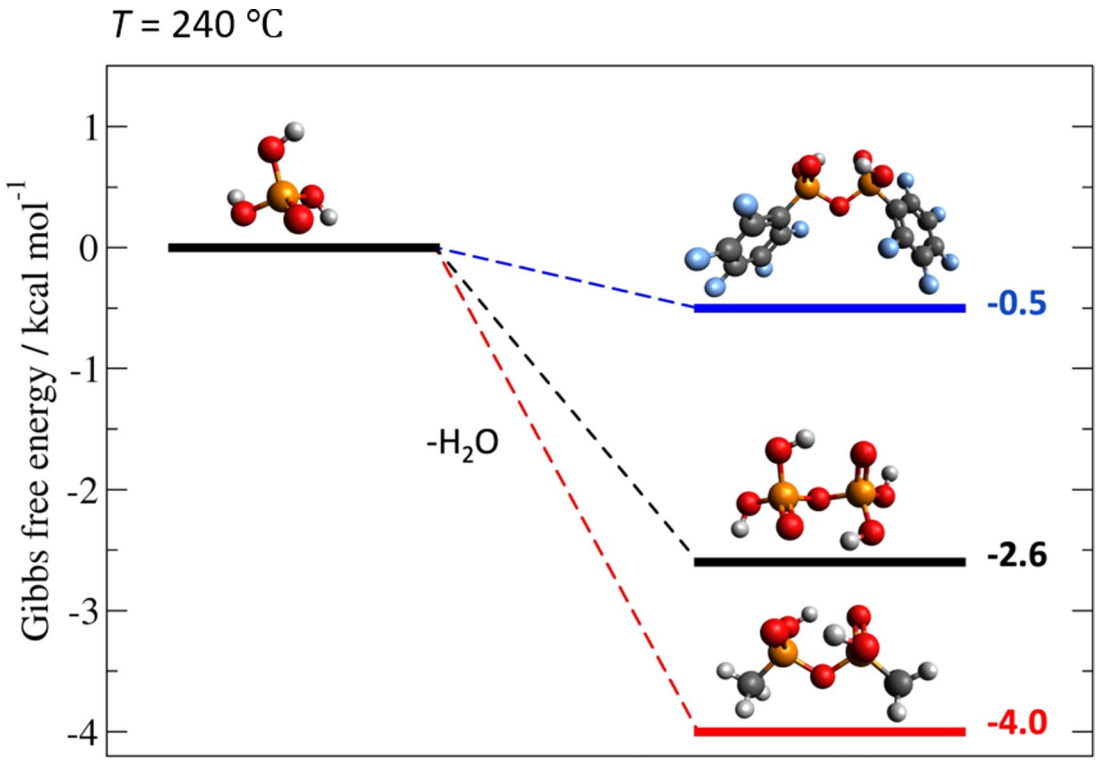

Extended Data Fig. 1 | Anhydride formation of phosphonic acid. Gibbs free energy diagrams for the anhydride formation at 240 °C: phosphoric (black), methylphosphonic (orange), and pentafluorophenylphosphonic acid (light blue).

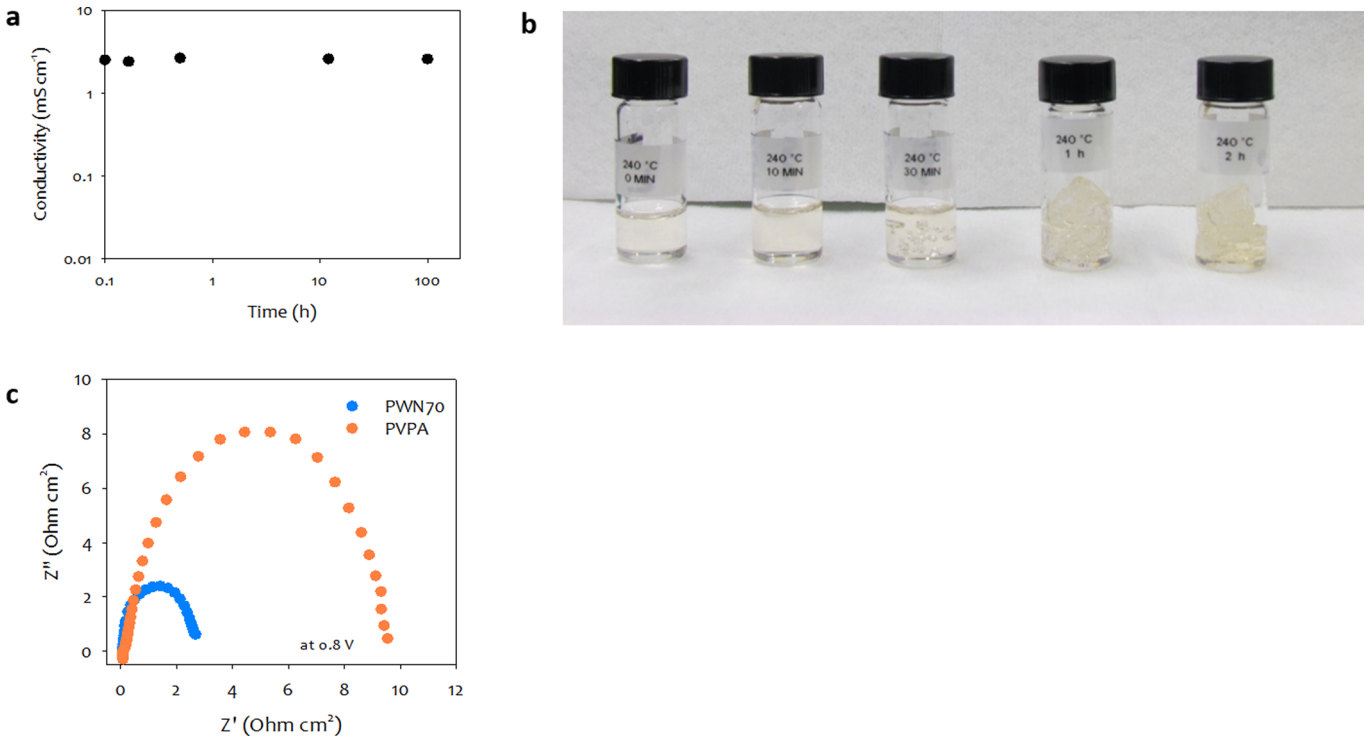

Extended Data Fig. 2 | Property change of PWN70 during high-temperature treatment. a, The conductivity change of PWN70 after exposure at 200 °C. The proton conductivity was measured in 5 wt.% DMSO solution at 80 °C. **b**, The solubility change of PWN70 after exposing at 240 °C. **c**, Electrochemical impedance analysis of PWN70 and PVPA MEAs at 160 °C. The impedance spectra were obtained at 0.8 V and a frequency range of 0.1 Hz to 1 MHz.

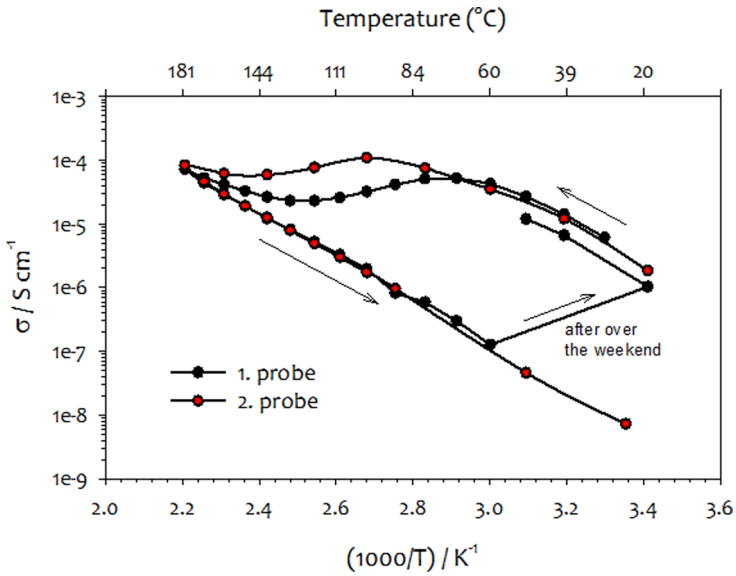

Extended Data Fig. 3 | Proton conductivity of PWN70 as a function of temperature. The conductivity was measured in an open system in ambient air (RH: ~35% at room temperature).

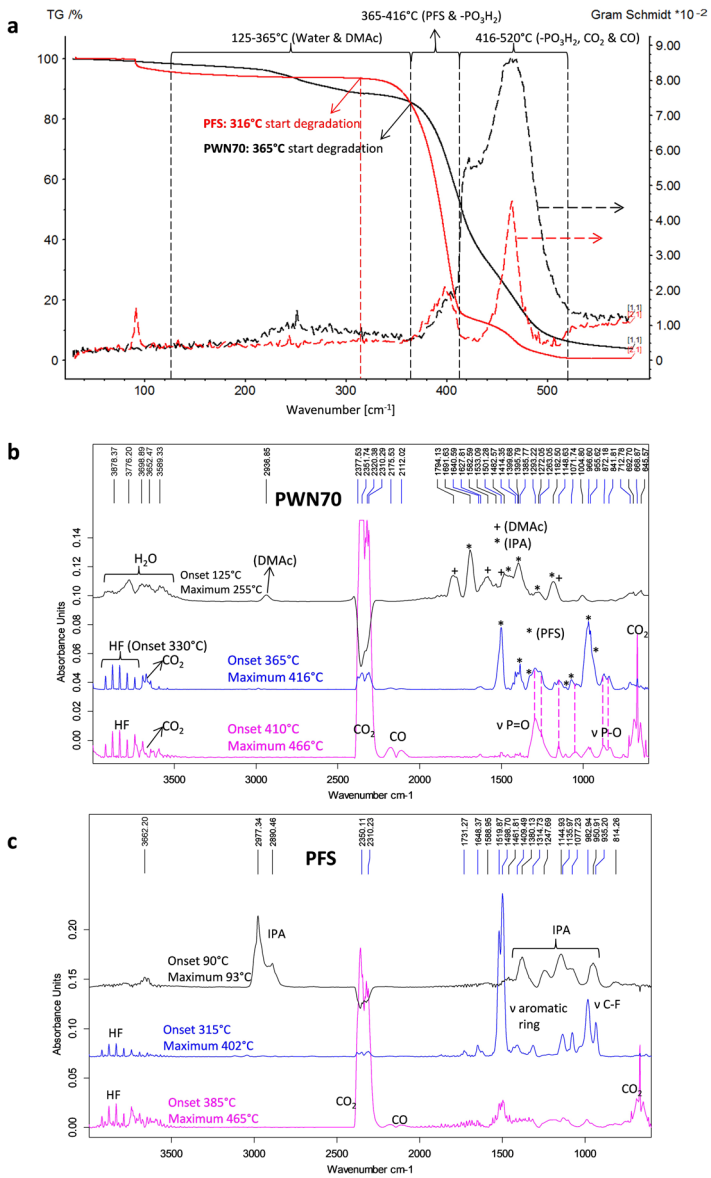

Extended Data Fig. 4 | Thermal oxidative stability of PWN70 and polypentafluorostyrene. a, TGA profiles (solid lines) and Gram Schmidt profiles (dashed lines) of PWN70 (black) and polypentafluorostyrene (red). **b**,**c**, FTIR spectra at selected temperatures for PWN70 (**b**) and for polypentafluorostyrene (**c**).

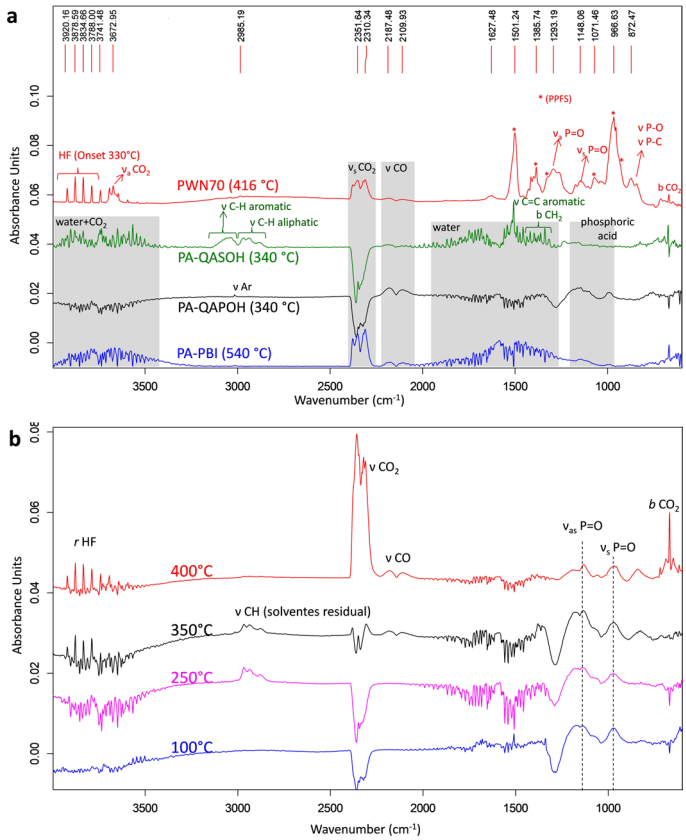

Extended Data Fig. 5 | FTIR spectra of proton conductors at selected temperatures. a, PWN70 (red), PA-QASOH (green), PA-QAPOH (black) and PA-PBI (blue) and **b**, TPP/Nafion composite as a function of temperature.

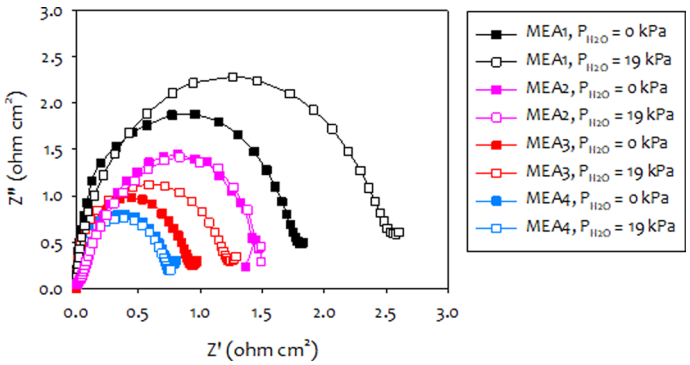

Extended Data Fig. 6 | Electrochemical impedance analysis of MEAs at 160 °C as a function of partial water vapour pressure. The impedance spectra were obtained at a frequency range of 0.1 Hz to 1 MHz.

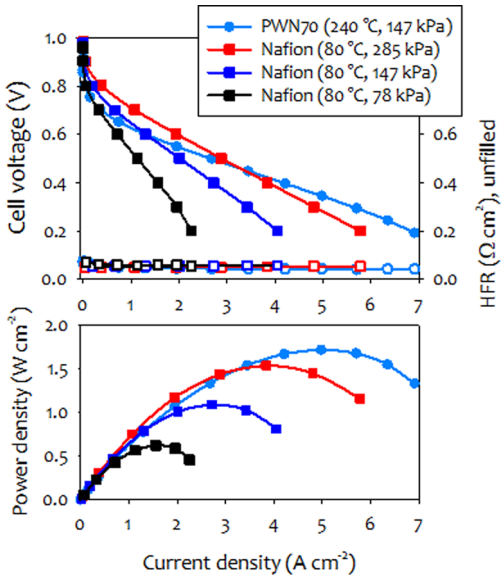

Extended Data Fig. 7 | Comparison of H_2/O_2 fuel cell performance between Nafion-based LT-PEMFC and PWN70-based HT-PEMFC. Nafion LT-PEMFC: cell temperature: 80 °C, membrane: Nafion 211 (25 μm thickness), Anode: Pt/C (0.6 mg_{Pt} cm^{-2}), Cathode: Pt/C (0.6 mg_{Pt} cm^{-2}), absolute backpressure varied from 78 to 285 kPa; PWN70-based HT-PEMFC: cell temperature: 240 °C, membrane: QAPOH–PA ion pair (40 μm thickness), Anode: PtRu/C (0.5 mg_{Pt} cm^{-2}), Cathode: Pt/C (0.6 mg_{Pt} cm^{-2}), absolute backpressure of 147 kPa.

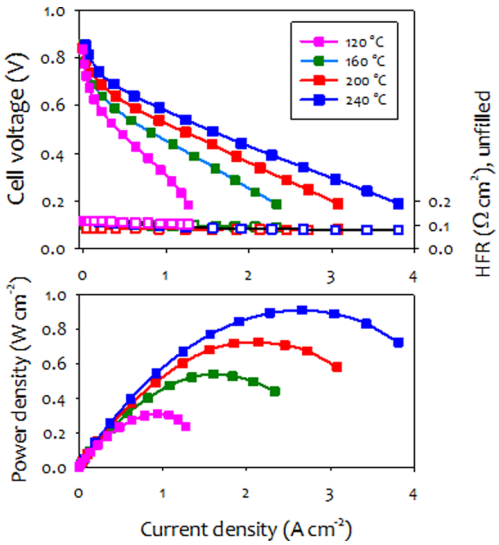

Extended Data Fig. 8 | H_2/air fuel cell performance of MEA4. The performance measured at 160, 200 and 240 °C under backpressure of 147 kPa. Membrane: QAPOH-PA ion pair (40 μm thickness), Ionomeric binder: PWN70, Anode: PtRu/C (0.5 mg_{Pt} cm^{-2}), Cathode: Pt/C (0.6 mg_{Pt} cm^{-2}).

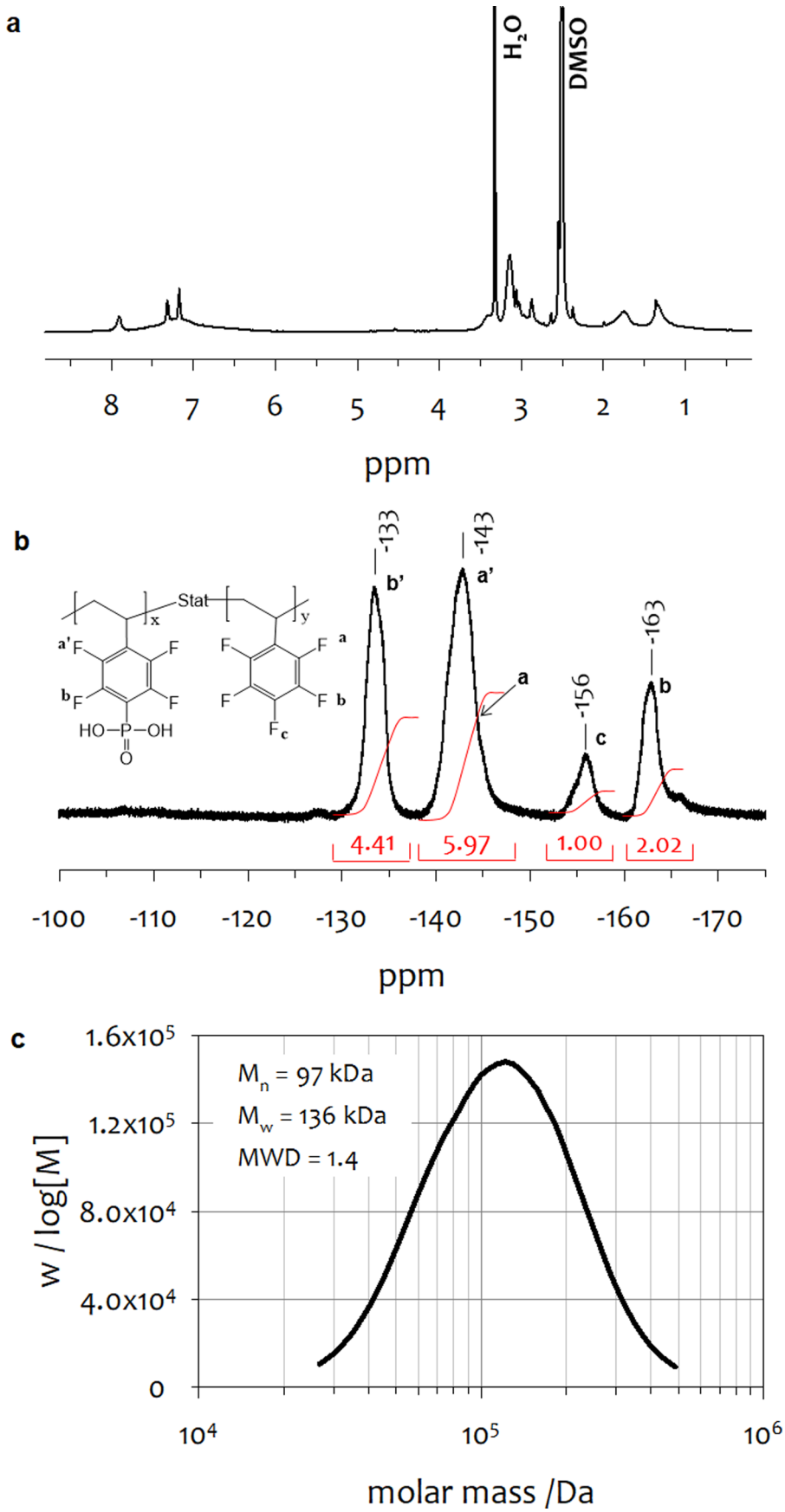

Extended Data Fig. 9 | See next page for caption.

Extended Data Fig. 9 | Structural characterization of polymers. a, ^{1}H NMR spectrum of QASOH in DMSO-d_6. **b**, ^{19}F NMR spectrum of PWN70 in DMSO-d_6, RT. The phosphonation degree calculated from ^{19}F NMR: 66–69 mol% and the phosphonation degree calculated from titration: 50 mol% (equivalent IEC = 2.21 mequiv. g^{-1}). ^{1}H-NMR (400 MHz, DMSO-d_6, ppm) δ = 8.36 (s, H), 4.33 (s, H), 3.77 (m, H), 2.94 (s, H), 2.78 (s, H), 1.95 (s, H), 1.02 (s, H) ^{19}F-NMR (250 MHz, DMSO-d_6, ppm) δ = −133.10 (bp 2 F), −143.14 (bp, 2 F). ^{31}P-NMR (101.2 MHz, DMSO-d_6, ppm) δ = -1.09 (bp,1 P). **c**, GPC profile of PWN70. Eluent: water, standard: PSSNa, detector: Shodex RI 101. M_n 97 kg mol^{-1}, M_w 136 kg mol^{-1}, PDI 1.40.

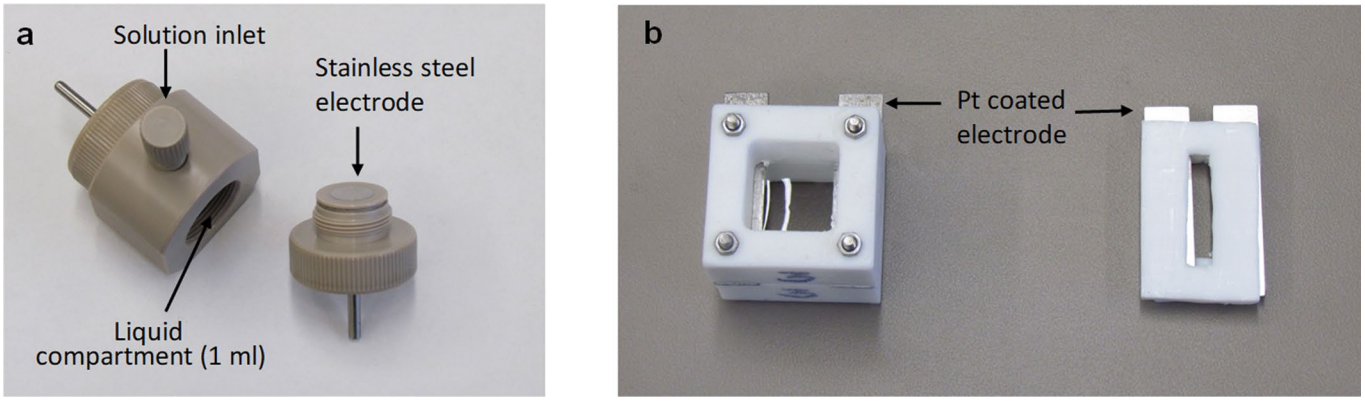

Extended Data Fig. 10 | Conductivity measurement cell. a, Liquid cell. **b**, Window cells for polymer film. Left: window opening: 2 cm; Right: window opening 0.5 cm.